



Universiteit
Leiden
The Netherlands

High-throughput mass spectrometric N-glycomics

Reiding, K.R.

Citation

Reiding, K. R. (2018, April 5). *High-throughput mass spectrometric N-glycomics*. Retrieved from <https://hdl.handle.net/1887/61076>

Version: Not Applicable (or Unknown)

License: [Licence agreement concerning inclusion of doctoral thesis in the Institutional Repository of the University of Leiden](#)

Downloaded from: <https://hdl.handle.net/1887/61076>

Note: To cite this publication please use the final published version (if applicable).

Cover Page



Universiteit Leiden



The handle <http://hdl.handle.net/1887/61076> holds various files of this Leiden University dissertation.

Author: Reiding, K.R.

Title: High-throughput mass spectrometric N-glycomics

Issue Date: 2018-04-05

Chapter 8

High-throughput serum *N*-glycomics: method comparison and application to study rheumatoid arthritis and pregnancy-associated changes

Research manuscript

Karli R. Reiding¹, Albert Bondt^{1,2†}, René Hennig^{3,4†}, Richard A. Gardner^{5†}, Roisin O'Flaherty^{6†}, Irena Trbojević-Akmačić^{7†}, Archana Shubhakar⁵, Johanna M. W. Hazes⁸, Udo Reichl^{3,9}, Daryl L. Fernandes⁵, Maja Pučić-Baković⁷, Erdmann Rapp^{3,4‡}, Daniel I. R. Spencer^{5‡}, Radboud J. E. M. Dolhain^{3‡}, Pauline M. Rudd^{6‡}, Gordan Lauc^{7,10‡}, Manfred Wuhrer^{1‡}

†These authors contributed equally

‡These authors contributed equally

¹Center for Proteomics and Metabolomics, Leiden University Medical Center (LUMC), Leiden, The Netherlands;

²Department of Rheumatology, LUMC, Leiden, The Netherlands;

³Max Planck Institute (MPI) for Dynamics of Complex Technical Systems, 39106 Magdeburg, Germany;

⁴glyXera GmbH., 39120 Magdeburg, Germany;

⁵Ludger Ltd., Culham Science Centre, Abingdon, Oxfordshire, United Kingdom;

⁶GlycoScience Group, National Institute for Bioprocessing Research and Training (NIBRT), Fosters Avenue, Blackrock, Co. Dublin, Ireland;

⁷Genos Glycoscience Research Laboratory, Zagreb, Croatia;

⁸Department of Rheumatology, Erasmus University Medical Center, Rotterdam, The Netherlands;

⁹Otto von Guericke University Magdeburg, Chair of Bioprocess Engineering, 39106 Magdeburg, Germany;

¹⁰Faculty of Pharmacy and Biochemistry, University of Zagreb, 10000 Zagreb, Croatia;

Manuscript under review.

8.1 Abstract

N-Glycosylation is a fundamentally important protein modification with a major impact on glycoprotein characteristics such as serum half-life and receptor interaction. More than half of the proteins in human serum are glycosylated, and the relative abundances of protein glycoforms often reflect alterations in health and disease. Several analytical methods are currently capable of analyzing the total serum *N*-glycosylation in a high-throughput manner.

Here we evaluate and compare the performance of released *N*-glycome analyses by hydrophilic-interaction ultra-high-performance liquid chromatography with fluorescence detection (HILIC-UHPLC-FLD), multiplexed capillary gel electrophoresis with laser-induced fluorescence detection (xCGE-LIF), and matrix-assisted laser desorption/ionization time-of-flight mass spectrometry (MALDI-TOF-MS) for analyzing the same panel of serum samples. The samples were obtained at multiple time points during the pregnancies and postpartum periods of healthy women and patients with rheumatoid arthritis (RA). We assessed the analytical methods based on their technical performance as well as on their ability to describe serum protein *N*-glycosylation changes throughout pregnancy, with RA, and with RA disease activity.

Overall, the methods proved to be similar in their detection and relative quantification of serum protein *N*-glycosylation. However, the non-MS methods showed superior repeatability over MALDI-TOF-MS, and allowed the best structural separation of low-complexity *N*-glycans. MALDI-TOF-MS achieved the highest throughput and provided compositional information on higher-complexity *N*-glycans. Consequentially, MALDI-TOF-MS could establish the linkage-specific sialylation differences within pregnancy and RA, whereas HILIC-UHPLC-FLD and xCGE-LIF demonstrated differences in α 1,3- and α 1,6-branch galactosylation. While the combination of methods proved to be the most beneficial for the analysis of total serum protein *N*-glycosylation, informed method choices can be made for the glycosylation analysis of single proteins or samples of varying complexity.

8.2 Introduction

Glycosylation is a critical and ubiquitous co- and post-translational protein modification which affects a wide variety of biological functions^{1,2}. Manipulation of protein *N*-glycosylation has shown to be effective for influencing protein half-life and receptor interaction in molecules as diverse as gamma-immunoglobulins (IgG) and alpha-immunoglobulins (IgA), as well as erythropoietin³⁻⁵. Furthermore, glycans of pathogens and cancer cells, as well as their receptors, are promising targets for both small molecule drugs and biopharmaceuticals⁶⁻⁸. Longitudinal studies have shown a remarkable stability of the total plasma protein *N*-glycome of individuals over a several-year period^{9,10}, while population studies have revealed associations of protein *N*-glycosylation with aging, sex, inflammation, body-mass index, metabolism, and a variety of cancers and autoimmune disorders¹¹⁻¹³. Longitudinal glycosylation profiling of single proteins and complex biofluids provides an opportunity for early detection of systemic alterations, and may serve to stratify patient populations¹⁴⁻¹⁶.

The last decade saw major developments in high-throughput (HTP) analytical methodologies for achieving *N*-glycosylation analysis^{17,18}. Of the methods available for glycan analysis, however, only a few have demonstrated the capability to profile the several thousands of samples making up many of the current-day clinical cohorts. The largest glycomics profiling studies thus far, all of them comprising more than 2000 cases, were performed with hydrophilic-interaction (ultra-)high-performance liquid chromatography with fluorescence detection (HILIC-(U)HPLC-FLD)¹⁹⁻²¹, multiplexed capillary gel electrophoresis with laser-induced fluorescence detection (xCGE-LIF)²², and matrix-assisted laser desorption/ionization (time-of-flight) mass-spectrometry (MALDI-(TOF)-MS)¹¹, and have assessed the released *N*-glycans from total serum/plasma or single glycoproteins such as IgG and alpha-1-antitrypsin. However, while each of the analytical methods proved informative for the analysis of *N*-glycosylation of complex-mixtures, none of them provided full structural characterization of glycan species without follow-up experiments such as exoglycosidase digestion and/or tandem-MS^{23,24}.

For glycans of relatively low complexity, such as found on the fragment-crystallizable (Fc) portion of IgG, comparative analysis has revealed highly similar findings between the aforementioned analytical methods²⁵⁻²⁷. However, the study of IgG-Fc glycosylation does not comprise structures of higher antennarity, *i.e.* tri- and tetraantennary species, nor the high levels of terminal *N*-acetylneuraminic acids found on most serum proteins other than IgG^{24,28}. In addition, many biological sources show more heterogeneous glycosylation than human IgG, and information on the comparative performance of HTP glycomics methods on such complex samples is still missing.

Here, we have studied the performance of the latest generation of HTP *N*-glycome analysis methodologies, focusing on HILIC-UHPLC-FLD, xCGE-LIF, and MALDI-TOF-MS. With this study we aimed to assess their respective suitability for total serum protein *N*-glycome (TSNG) analysis, explore the overlap and orthogonality of the information between the methods, and determine their strengths and weaknesses for revealing different types of *N*-glycan properties. To answer these questions in a clinically relevant setting, all methods were challenged with analyzing the same subset of the pregnancy-induced amelioration of rheumatoid arthritis (PARA) cohort, a longitudinal study aimed at exploration of the temporary improvement of rheumatoid arthritis (RA) severity experienced by women during pregnancy²⁹.

Table 1. Characteristics of pregnancies included in the study.

	Pregnancies	
	Control (n = 32)	RA (n = 36)
Age at delivery in years, mean (SD)	32.1 (4.4)	32.5 (4.0)
Duration of pregnancy in weeks, mean (SD)	40.1 (1.4)	39.2 (1.9)
Disease duration at first visit in years, mean (SD)	-	7.3 (5.8)
ACPA positive patients, n (%)	-	22 (61%)
RF positive patients, n (%)	-	25 (69.4%)
Erosive disease, n (%)	-	14 (38.9%)
Disease activity score (DAS28(3)-CRP) at preconception, mean (SD)	-	3.8 (1.0)

Table 2. Participating laboratories and methodologies used in the study.

Affiliation (participant)	Methodology	Labeling or modification	Clean-up	Automation	Annotation	References
NIBRT (1)	HILIC-UHPLC-FLD	2-AB labeling	Solid-phase hydrazide bead capture; Hypersep Diol cartridge	sample preparation	GU value with database	23,41
Genos (2)	HILIC-UHPLC-FLD	2-AB labeling	GHP filter plate	-	GU value with database	23,41
Ludger (3)	HILIC-UHPLC-FLD	2-AB labeling	LudgerClean T1 cartridge	sample preparation	GU value with database; LC-MS composition analysis	66
MPI (4)	xCGE-LIF	APTS labeling	glyXera glyXbeads	normalization; integration; database matching; quality control	Normalized migration time value with database	10,31,61
LUMC (5)	MALDI-TOF-MS	Ethyl esterification of sialic acids	GHP filter plate	sample preparation; integration; quality control	mass error; isotope distribution	35,40

8.3 Results

To qualitatively compare glycomics analytical methodologies, we measured the released TSNGs of 36 RA patient pregnancies at three time points (before conception, at the 3rd

trimester of pregnancy, and 26 weeks postpartum) and 32 pregnancies of healthy controls at two time points (at the 3rd trimester, and 26+ weeks postpartum) (**Table 1**). In addition, a repeat measurement of a standard plasma sample was included in the study to establish intra- and interplate variation. The methodologies used on the released glycan samples were as follows: HILIC-UHPLC-FLD after 2-aminobenzamide (2-AB) labeling, xCGE-LIF after 8-aminopyrene-1,3,6-trisulfonic acid (APTS) labeling, and MALDI-TOF-MS after ethyl esterification of the sialic acids (**Table 2**). The HILIC-UHPLC-FLD analysis was performed by three independent laboratories applying their standard protocols (**Supplemental Methods**).

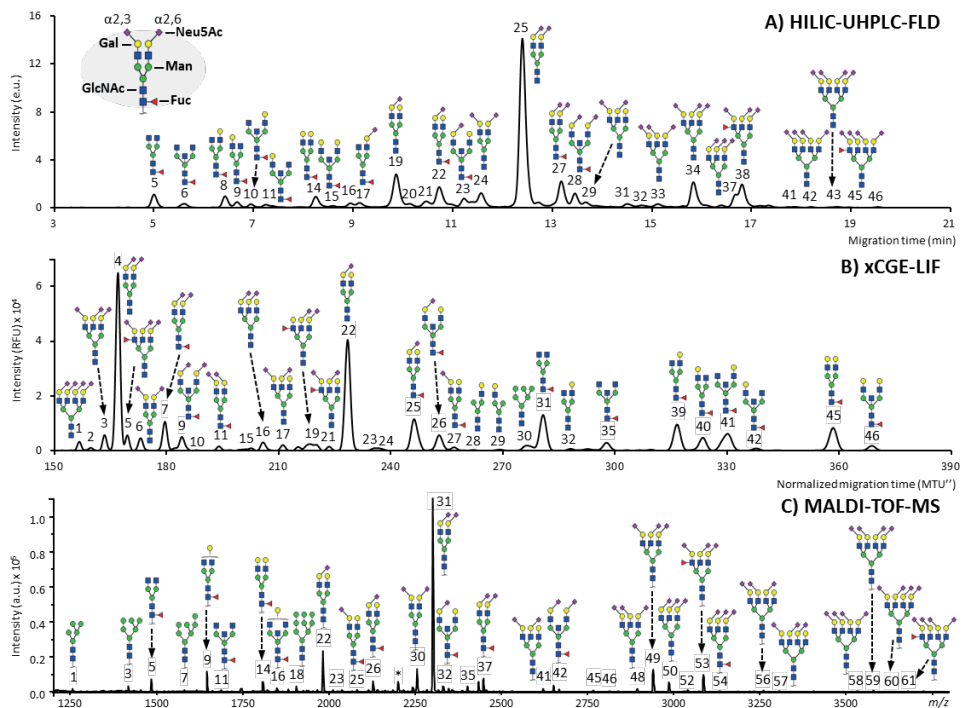


Figure 1. The respective profiles of the same total plasma protein N-glycan standard as recorded by HILIC-UHPLC-FLD, xCGE-LIF and MALDI-TOF-MS. **A)** Chromatogram as obtained by HILIC-UHPLC-FLD after 2-AB labeling. **B)** Electropherogram as obtained by xCGE-LIF after APTS labeling. **C)** Mass spectrum as obtained by MALDI-TOF-MS after ethyl esterification, with species assigned as $[M+Na]^+$. Signals of all recordings have been annotated to the best of knowledge, making use of the detections across the methods as well as established literature on biochemical pathways and plasma/serum N-glycosylation. The display of linkage has been restricted to the N-acetylneuraminic acids (sialic acids), which was principally acquired by MALDI-TOF-MS. Branching differences (galactose arm, bisection, fucose position) were only distinguishable by HILIC-UHPLC-FLD and xCGE-LIF. For full assignments of the signals see **Supplementary Tables S1, S2, and S3**, as well as **Supplementary Figure S1**.

Signal detection

HILIC-UHPLC-FLD allowed the integration of 46 signals, with peak identities inferred by matching standardized retention times *via* GU values to database entries (**Supplemental Table S1**)³⁰. xCGE-LIF enabled the integration of 49 signals, and peak identity was inferred by matching migration times *via* database entries (**Supplemental Table S2**)³¹. For MALDI-TOF-MS, 61 signals were detected that passed the established quality criteria (**Supplemental Figure S1; Supplemental Table S3**). The analyses broadly detected the same *N*-glycan species, with some variation per method in structural and compositional overlap (**Supplemental Table S4**), and the assignments were in line with previously established serum and plasma *N*-glycosylation features³²⁻³⁴.

All analytical methods showed comparable results in their representation of the overall serum and plasma profile (**Figure 1**). Clearly defined for all methods were the two largest signals belonging to A2G2S[6,6]2 (H5N4E2, for HILIC-UHPLC-FLD, xCGE-LIF and MALDI-TOF-MS peaks 25, 4, and 31, respectively) and A2G2S[6]1 (H5N4E1, peaks 19, 22, and 22) (**Supplemental Table S4**). In addition, all methods demonstrated the high-definition detection of asialylated diantennary glycans, *e.g.*, FA2 (H3N4F1, peaks 5, 31, 5), and FA2G2 (H5N4F1, peaks 14, 45, 14). However, the non-MS methods allowed distinction between the galactose-linkage sites of the monogalactosylated species, *e.g.*, FA2[3]G1 (peaks 8, 39, -) and FA2[6]G1 (peaks 9, 40, -), whereas MALDI-TOF-MS could only detect the common composition belonging to these structures, namely H4N4F1 (peak 9). Similarly, while the presence of a bisecting *N*-acetylglucosamine led to unique retention/migration times, the corresponding mass spectrometric compositions also apply to triantennary structures with incomplete galactosylation. For example, the MALDI-TOF-MS composition H3N5F1 could align to FA2B (peaks 6, 35, 11) or FA3 (not detected), although these are not commonly found in high abundance in human serum^{24,28}. On the other hand, mass spectrometry proved capable of individually detecting different sizes of high-mannose and hybrid-type *N*-glycans, whereas these species overlapped with diantennary glycans in the non-MS methods (**Supplemental Table S4**).

The two main species belonging to the triantennary structures were also detected by all analyses, *i.e.*, A3G3S[3,6,6]3 (H6N5L1E2, peaks 34, 3, 49) and A3F1GS[3,6,6]3 (H6N5F1L1E2, peaks 38, 5, 53). However, while the specific sialic acid linkage variants of the triantennary glycan compositions could be discriminated by MALDI-TOF-MS, *e.g.*, H6N5L3, H6N5L2E1, H6N5L1E2 and H6N5E3, the accompanying structures could not clearly be assigned to individual signals for HILIC-UHPLC-FLD and xCGE-LIF without additional steps of linkage-specific enzymatic removal of the sialic acids and sample re-measurement. This situation was similar for the tetraantennary compositions.

Based on the structural information and separation achieved by the various methods, we constructed a series of derived traits to describe single glyco-enzymatic steps and presumed protein-specific glycosylation patterns (**Supplemental Tables S5 and S6**)^{28,35}.

Method repeatability

All methods showed robust detection of the plasma standard analyzed in 10 replicates, with UHPLC generally displaying the least variation and MALDI-TOF-MS the most (**Supplemental Figure S2 and Supplemental Table S7**). Specifically, the main peak (A2G2S[6,6]2 or H5N4E2) showed for HILIC-UHPLC-FLD a coefficient of variation (CV) of 1.9% (participant 2, which displayed the lowest variation among the UHPLC methods), for xCGE-LIF of 5.1% and for MALDI-TOF-MS of 5.8%. Further examples include the CVs of FA2 (H3N4F1) respectively being 1.7%, 13.8%, and 17.7%, and of A3G3S[3,6,6]3 being 0.9%, 10.3%, and 13.2%. Overall, the average CVs of the 10 most abundant peaks for each method were 1.6%, 6.9% and 11.5%. For MALDI-TOF-MS most derived traits showed a higher repeatability than the individual peaks making up the traits, exemplified by the 50 most abundant traits having a mean CV of 2.6%, while for the non-MS methods the CVs of derived traits remained similar to their constituent peaks.

Intermethod signal correlation

Using the clinical cohort data, we could explore which signals displayed similar behavior across the orthogonal methods. To achieve this, Pearson correlation coefficients were calculated between the methods for all single signals (**Figure 2**), as well as for the derived traits (**Supplemental Figures S3, S4, S5 and S6**). Note that the correlations obtained in this manner are the result of similarity of *N*-glycan behavior across pregnancy, RA and disease activity thereof, as well as of other biological and technical sources of variation that were unaccounted for in this study. As such, positive correlation within and between methods occurred when signals contained the same glycan structure (single isolated hit), or when different glycans underwent the same enzymatic modification (multiple hits sharing a single property such as antennary fucosylation). Negative correlation could similarly arise due the relationship between enzymatic substrates and products (*e.g.*, the process of galactosylation induces negative correlation between galactosylated and nongalactosylated species) and protein-abundance changes (*e.g.*, an increase in all diantennary species such as present on immunoglobulins will lead to a relative decrease in all tri- and tetraantennary glycans).

Between the UHPLC methods a good correlation was observed for peaks containing the same glycans, examples being peak 5 (FA2, mean $r = 0.90$ SD ± 0.07), peak 27 (FA2G2S[6,6]2, $r = 0.93 \pm 0.01$) and peak 34 (A3G3S[3,6,6]3, $r = 0.90 \pm 0.02$) (**Supplemental Figure S4A-C**). Signals with lower correlation across the methods were generally of low intensity. Strong correlation of the aforementioned signals was also visible with the corresponding xCGE-LIF annotation, *i.e.*, UHPLC peak 5 with xCGE-LIF peak 31 (FA2; $r = 0.96$), 27 with 7

(FA2G2S[6,6]2, $r = 0.87$), and 34 with 3 (A3G3S[3,6,6]3, $r = 0.88$) (**Supplemental Figure S4D**). Next to single signals, the derived traits showed to be highly comparable between methods as well (**Supplemental Figure S5**).

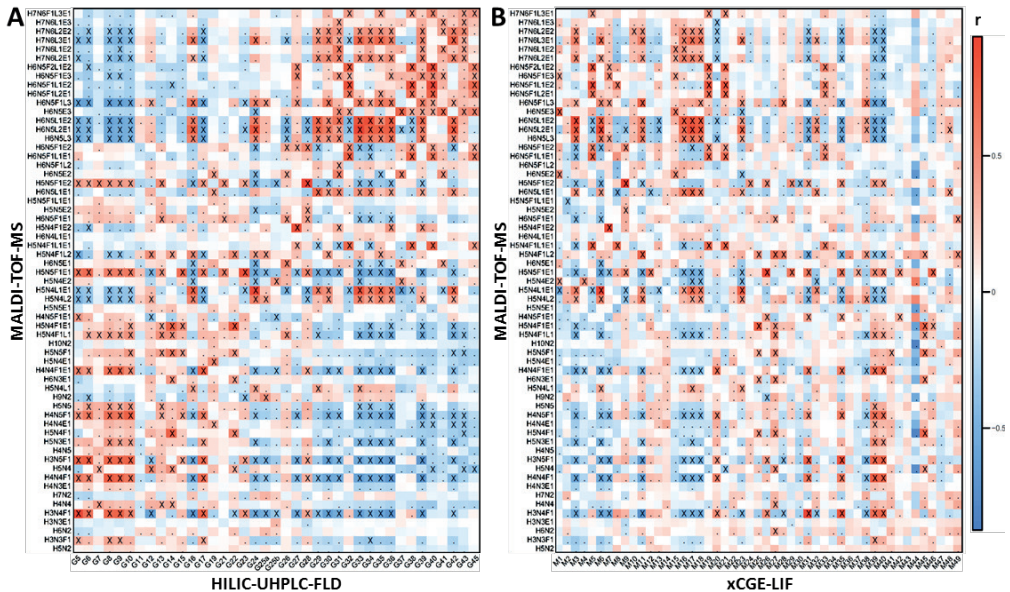


Figure 2. Heat map visualizing the Pearson correlation between signals from MALDI-TOF-MS, HILIC-UHPLC-FLD (participant 2) and xCGE-LIF. **A)** HILIC-UHPLC-FLD (horizontal) with MALDI-TOF-MS (vertical). **B)** xCGE-LIF (horizontal) with MALDI-TOF-MS (vertical). Signal correlations were calculated on clinical data, and represent similarity of behavior with biological phenotypes such as pregnancy and RA as well as technical variation. Crosses (X) indicate correlations significant below a p -value of $1 \cdot 10^{-5}$, whereas dots (.) indicate correlation below a p -value of 0.05. For similar heat maps between non-MS methods and derived traits see **Supplementary Figures S4, S5, and S6**. H = hexose, N = N-acetylhexosamine, F = deoxyhexose (fucose), L = (lactonized) α 2,3-linked N-acetylneuraminic acid, E = (ethyl esterified) α 2,6-linked N-acetylneuraminic acid.

Complementarity of methods for signal assignment

When comparing the signals of the non-MS methods with MALDI-TOF-MS, an advantage of analyzing the sample set with two vastly orthogonal methods becomes apparent (**Figure 2**). For instance, in several cases ambiguously annotated non-MS signals could be attributed to specific glycan structures by making use of the correlation with MS. One example hereof is chromatographic peak 28, which, while theoretically encompassing FA2BG2S[6,6]2, FA2BG2S[3,6]2 and FA2BG2S[3,3]2, strongly correlated with MALDI-TOF-MS composition H5N5F1E2 (FA2BG2S[6,6]2, $r = 0.92$), and to a much lesser degree with H5N5F1L1E1 (FA2BG2S[3,6]2, $r = 0.27$) and H5N5F1L2 (FA2BG2S[3,3]2, not detected) (**Figure 2A, Supplemental Figure S3**). Similarly, by correlation xCGE-LIF peak 1 is likely to contain H6N5E3 (A3G3S[6,6,6]3, $r = 0.68$), even though this was not principally annotated for the

electrophoretic signal (**Figure 2B**). On the other hand, structural characteristics could be attributed to MALDI-TOF-MS compositions on basis of the assignments from the non-MS methods. For instance, the fucosylated triantennary compositions with at least one α 2,3-linked sialic acid correlated strongly with antennary-fucosylated but not with core-fucosylated structures, *e.g.*, H6N5F1L1E2 with UHPLC peak 38 and xCGE-LIF peak 5 (A3F1G3S[3,6,6]3, respectively $r = 0.86$ and $r = 0.82$), and not with UHPLC peak 36 (FA3G3S[3,6,6]3, $r = 0.10$). While core-fucosylated structures are still likely present in the MALDI-TOF-MS composition, it does appear that the main differences observed within the cohort originated instead from antennary fucosylation.

Next to single glycans, derived traits showed good overlap between MS and non-MS methods, but a larger set of these could be constructed for MS due to the unambiguous compositional assignment of signals (**Supplemental Figure S6**).

Association with pregnancy and RA

Within the PARA study, we compared for the different methods the glycosylation changes observed throughout pregnancy (assessed at preconception, the 3rd trimester of pregnancy, and 26+ weeks postpartum), between healthy controls and RA patients, as well as the association with RA disease activity as expressed by the DAS28(3)-CRP value. The comparability between methods was assessed by the effect directions of the significant findings from mixed model regression analyses, and are represented as box- and scatterplots (**Figure 3**). For all analyses, glycosylation parameters were centered to zero and scaled to represent single SD changes. Effects were deemed significant under a study-wide false-discovery rate of 5% (leading to a threshold $\alpha = 1.7 \cdot 10^{-2}$).

Pregnancy showed to have a major effect on the TSNG, and congruent effects were observed by all methods (**Supplemental Table S8**), both for the single glycans (**Figure 3A**) and derived traits (**Figure 3B**). Notable examples included the decrease of FA2 with pregnancy, as seen for HILIC-UHPLC-FLD (participant 2 throughout) peak 5 ($\beta = -2.32 \text{ SE} \pm 0.38$), xCGE-LIF peak 31 ($\beta = -2.37 \pm 0.39$) and MALDI-TOF-MS composition H3N4F1 ($\beta = -2.34 \pm 0.43$), and the consequentially increased overall galactosylation of (nonsialylated) diantennary fucosylated species representative of IgG-Fc (A2FS0G, respectively, $\beta = 1.62 \pm 0.27$, $\beta = 1.92 \pm 0.31$, and $\beta = 1.67 \pm 0.28$)²⁸. Likewise, all methods indicated a profound decrease in bisection of sialylated diantennary species, likely representative of non-IgG-Fc immunoglobulin glycosylation (A2FSB, $\beta = -3.10 \pm 0.48$, $\beta = -1.55 \pm 0.26$, and $\beta = -1.81 \pm 0.29$)²⁸.

Interestingly, one of the major *N*-glycan species to change with pregnancy, namely the fully α 2,3-sialylated A3F1G3S[3,3,3]3, was only uniquely separable as the MALDI-TOF-MS composition H6N5F1L3 ($\beta = 1.61 \pm 0.26$), but likely also drove the changes in the ambiguously assigned UHPLC signal 33 ($\beta = 2.92 \pm 0.43$) and xCGE-LIF signal 3 ($\beta = 1.31 \pm$

0.24). However, due to overlap in retention and migration times, the derived trait for α 2,3-linked sialylation on triantennary species (A3GL) could only be established for MALDI-TOF-MS ($\beta = 2.57 \pm 0.40$) (**Figure 3C**). HILIC-UHPLC-FLD, on the other hand, uniquely showed with pregnancy a strong difference in the galactose position of monogalactosylated and bisected diantennary *N*-glycan species (e.g., relative 6-arm galactosylation, FA2[r6]BG1, $\beta = -9.41 \pm 2.42$), whereas xCGE-LIF could uniquely detect a change in GlcNAc position of monoantennary species (e.g., relative 6-arm GlcNAc position, A1[r6]G1, $\beta = 1.96 \pm 0.31$).

Differences between RA patients and healthy controls proved less pronounced than the differences during pregnancy, but were similarly detected across methods. Mixed logistic regression was used for the comparison of glycosylation parameters with RA (healthy = 0, RA = 1), correcting for pregnancy by modelling a random intercept per time point (**Supplemental Table S9**). RA patients showed to have a lower galactosylation of glycans commonly found on IgG-Fc (A2FS0G, for HILIC-UHPLC-FLD $\beta = -1.89 \pm 0.36$, for xCGE-LIF $\beta = -1.85 \pm 0.36$, and for MALDI-TOF-MS $\beta = -1.78 \pm 0.36$), and higher bisection of sialylated fucosylated diantennary species (A2FSB, $\beta = 1.25 \pm 0.31$, $\beta = 0.53 \pm 0.21$, and $\beta = 0.88 \pm 0.26$) (**Figure 3B**). Also detected by HILIC-UHPLC-FLD and MALDI-TOF-MS was a higher bisection with RA of afucosylated nonsialylated diantennary species (A2F0S0B, respectively $\beta = 1.11 \pm 0.28$, and $\beta = 0.69 \pm 0.20$). Absent from MALDI-TOF-MS but present for the non-MS methods were differences in branching for lower complexity *N*-glycans, namely for HILIC-UHPLC-FLD the relative 6-branch galactosylation of monogalactosylated and sialylated diantennary species with bisection (FA2[r6]BG1S1, $\beta = -0.90 \pm 0.30$) and for xCGE-LIF the antennary-branch of monoantennary species (A1[r6]G1, $\beta = -1.05 \pm 0.28$) (**Figure 3C**).

Lastly, linear regression was used to model the association of glycosylation (independent) with DAS28(3)-CRP (dependent). In addition, mixed linear regression was used with either a random intercept per individual to assess the association throughout pregnancy, or with a random intercept per time point to assess the association between individuals. These different models provided highly congruent findings (**Supplemental Table S10**). In all, for each method a strong negative association was seen between DAS28(3)-CRP and IgG-Fc-type galactosylation (A2FS0G, HILIC-UHPLC-FLD $\beta = -0.51 \pm 0.11$, xCGE-LIF $\beta = -0.51 \pm 0.11$, MALDI-TOF-MS $\beta = -0.50 \pm 0.11$) (**Figure 3D**). Increased with disease activity proved to be the fucosylation of triantennary structures (A3F, $\beta = 0.50 \pm 0.11$, $\beta = 0.33 \pm 0.12$, and $\beta = 0.38 \pm 0.12$), as well as the sialylation thereof (A3S, $\beta = 0.52 \pm 0.11$, A3FS $\beta = 0.23 \pm 0.12$ (trend), and A3FGS, $\beta = 0.41 \pm 0.12$). MALDI-TOF-MS analysis specifically showed that the increases in fucosylation and sialylation were similar for the tri- and tetraantennary species (e.g., A4FE, $\beta = 0.42 \pm 0.12$), and revealed that there were no sialic acid linkage-biases in these increases (e.g., A3EF, $\beta = 0.39 \pm 0.12$ vs. A3LF, $\beta = 0.40 \pm 0.12$). HILIC-UHPLC-FLD, on the other hand, was again able to detect significant branching differences with changing

disease activity (FA2[r6]G1S1, $\beta = -0.34 \pm 0.12$), while xCGE-LIF showed higher resolution for the monoantennary species (*e.g.*, A1F, $\beta = 0.48 \pm 0.14$).

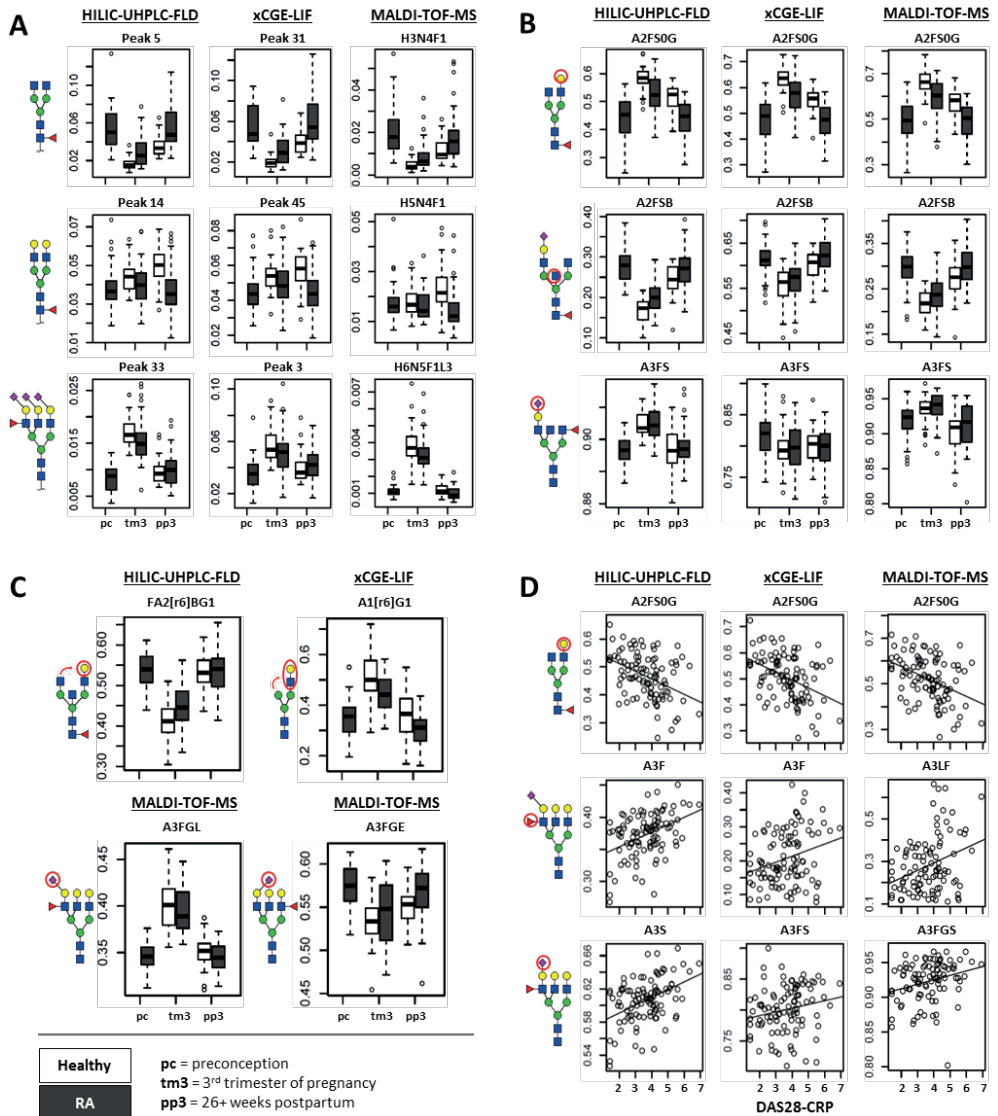


Figure 3. Comparability of HILIC-UHPLC-FLD (participant 2) (left), xCGE-LIF (middle) and MALDI-TOF-MS (right) for the detection of clinical characteristics of pregnancy, RA and RA disease activity. **A)** Comparability of single glycan signals (% area) with pregnancy (preconception = pc, 3rd trimester of pregnancy = tm3, 26+ weeks postpartum = pp3) and RA (healthy = white, RA = grey). **B)** Comparability of derived glycosylation traits with pregnancy and RA. **C)** Derived trait differences detected uniquely by a single method with pregnancy and RA. **D)** Association of derived glycosylation traits with RA disease activity (DAS28-CRP). For a legend of the derived traits see **Supplementary Table S6**.

8.4 Discussion

Previous method comparisons involved the analysis of released *N*-glycans and glycopeptides of single proteins, examples being IgG and prostate-specific antigen (PSA)^{25-27,36}. In our comparative study we have instead focused on the analysis of released *N*-glycans from the total pool of serum glycoproteins, which principally allows the detection of a larger variety of systemic abnormalities than would be possible from a single protein, but also displays *N*-glycosylation of considerably higher complexity^{24,28,37}.

We included in our comparison analytical methodologies that have displayed the throughput capacity for several thousands of serum *N*-glycome samples, as currently the case for HILIC-UHPLC-FLD, xCGE-LIF and MALDI-(TOF-)MS^{11,19,20,22}. Technical considerations for these studies include analyte stability, preparation- and measurement-throughput, as well as software solutions for the integration and analysis of the consequentially large datasets, all of which have been demonstrably addressed for the indicated techniques. To appreciate the technical possibilities and constraints of the methods, their mechanisms of separation need to be considered. 1) HILIC-UHPLC-FLD separates glycan structures on basis of their hydrophilic interaction with a stationary phase, generally meaning that larger structures, as well as those with larger surface areas or charged *N*-acetylneuraminic acids, have increased retention times³⁸. 2) In xCGE-LIF glycans are separated along an electric field inside a polymer-filled capillary, according to their mass/charge (*m/z*) ratio and their size/shape (hydrodynamic diameter). Analytes with lower *m/z* (higher charges and/or lower masses) migrate faster through the capillary than those with higher *m/z*^{10,39}. 3) MALDI-TOF-MS separates ionized glycans (here [M+Na]⁺) by *m/z* ratio, with the esterification procedure employed to stabilize sialic acids, to prevent unfavorable negative charges on the sialylated species and to introduce an MS-detectable mass difference between α 2,3- (lactonized) and α 2,6-linked (ethyl esterified) sialic acids⁴⁰.

In this comparison study, we judged the relative performance of the HTP TSNG methods on the basis of technical replicate measurements, as well as by a set of samples from a longitudinal study on the improvement of disease activity within RA patients during pregnancy²⁹.

Throughput and repeatability

Sample preparation throughput proved similar between the methods, each of them requiring (overnight) enzymatic *N*-glycan release, 1 – 2 h chemical derivatization at either the glycan reducing end or at the sialic acid, and HILIC solid-phase extraction (SPE) prior to analysis. Automated sample preparation was reported for both the HILIC-UHPLC-FLD and MALDI-TOF-MS workflows^{35,41}, but the congruencies in protocols suggest that xCGE-LIF could make use of similar strategies. Aside from sample preparation, MALDI-TOF-MS showed to have highest analytical throughput with an approximate throughput of 10 s per

sample, whereas xCGE-LIF and UHPLC runs required 40 min to an hour. A major advantage for xCGE-LIF is the multiplexing capability (with up to 96 capillaries in parallel) allowing the simultaneous analysis of up to 96 samples, which reduces the effective analysis time per sample to less than 30 seconds.

The most repeatable method proved to be HILIC-UHPLC-FLD (albeit with variation between participants), whereas MALDI-TOF-MS showed the most technical variation. Interestingly, although the lower repeatability of the MALDI-TOF-MS method did indeed lead to larger SDs on the biological effects as well as a consequential decrease in statistical significance (an increase in *p*-value) by typically one or more orders of magnitude, in practice very few findings were rejected in this study due to lack of statistical power. As such, the lower repeatability of MALDI-TOF-MS does not appear to hamper the glycomics analyses of larger cohorts, but the repeatability of the non-MS methods would definitely be of benefit for the quantification of small effect sizes.

Of interest, while MALDI-TOF-MS repeatability was higher for the derived traits, which often are groupings of chemically similar *N*-glycan species, no such improvement was observed for either HILIC-UHPLC-FLD or xCGE-LIF. This would suggest presence of an MS-specific component of measurement error, possibly relative ionization efficiency or response linearity, both of which could be controlled for with the use of internal standards^{42,43}.

Analyte separation and annotation

Whereas MALDI-TOF-MS does principally not separate all *N*-glycans but only those with differing chemical compositions, both HILIC-UHPLC-FLD and xCGE-LIF produce unique standardized retention times, respectively migration times, for glycans with different structures. However, while the MS analysis provided the resolution to separate the majority of possible compositions, for the non-MS methods a large portion of glycan structures were not separated from other analytes. Accordingly, only HILIC-UHPLC-FLD and xCGE-LIF were capable of revealing additional features in the low-complexity (IgG-Fc) regions of their chromatograms or electropherograms for the analyses of the TSNG, e.g. *N*-acetylglucosamine linkage (antennary or bisecting), galactose position (α 1,3 or α 1,6 branch), and fucose position (core or antennary). On the other hand, MALDI-TOF-MS proved the most informative for larger glycan structures (e.g. tri- and tetraantennary species), for instance on the exact number of LacNAc units (antennarity), the number of fucoses, and the number and linkage of *N*-acetylneuraminic acids. To generalize, in profiling mode HILIC-UHPLC-FLD and xCGE-LIF appeared optimal for high-density structural identification of a low-complexity sample, e.g., immunoglobulin glycosylation, be it from blood or most of the commonly used recombinant production systems, whereas MALDI-TOF-MS appeared preferentially suitable for the analysis of samples with high-complexity and/or larger *N*-glycan species.

Each of the described methods may obtain additional structural information on the glycans by including more experimental dimensions. One can think of on-line hyphenation of separation techniques, examples including LC-MS(/MS), CE-MS(/MS), and ion-mobility MS⁴⁴⁻⁴⁶, or off-line approaches such as exoglycosidase digestion²³. While increasing the information content, these added dimensions also drastically increase analysis times and data complexity, and have thus far only been reported for relatively small sample sets. However, with the advancements in development of rapid glycan preparations protocols, laboratory automation and evolution of big data analysis methods, the idea of HTP laboratories employing these innovative approaches in glycan analysis of larger sample sets on different glycoprotein levels might not be too far way. Today, more commonly achieved for HTP applications is the thorough structural annotation of one or a few samples, with the expectation that these are representative for the set, as is for instance achieved with exoglycosidase digestion or MS/MS experiments^{23,24}. Interestingly, our study suggests that parallel glycomics analysis by orthogonal HTP methods as well allows the determination of many of the sample-relevant structural characteristics, without necessarily including a step of throughput-limiting serial hyphenation. A prominent example of this is the structure FA2BG2S2 correlating with composition H5N5F1E2, for which HILIC-UHPLC-FLD and xCGE-LIF determined the core-fucosylation and bisection while MALDI-TOF-MS determined the α 2,6-linkage of the *N*-acetylneuraminic acids (**Supplemental Figure S3B and C**).

Clinical observations

Associations found between *N*-glycosylation and pregnancy, RA and RA disease activity (DAS28(3)-CRP) were very much in line with previous TSNG studies⁴⁷⁻⁴⁹(**Chapter 7**), and agreed with reports on single glycoproteins dominant in human serum⁵⁰⁻⁵³. Main findings with pregnancy included an increased antennarity, nonsialylated FA2 galactosylation, and α 2,3-linked sialylation as well as a decreased bisection of sialylated FA2. Individuals with RA proved to have on average a lower FA2 galactosylation and higher bisection compared to their healthy counterparts, and disease activity of RA associated positively with A3/A4 for both fucosylation and sialylation (without particular preference in linkage), and negatively with the galactosylation of FA2.

As with all analyses of the released TSNG, the here-reported differences may originate from changes in protein glycosylation, or from differences in the relative abundances of glycoproteins in serum. Nonetheless, the changing glycosylation phenotypes seem to reflect immune modulation of either IgG-Fc (predominantly nonsialylated FA2)^{28,51}, IgG-Fab and other plasma-cell-derived immunoglobulins (highly sialylated FA2)^{28,51}, or acute phase glycoproteins such as alpha-1-antitrypsin and alpha-1-acid glycoprotein (tri- and tetraantennary species)^{28,52,54,55}. In addition, the previously reported MALDI-TOF-MS association of A3FGS with DAS28(3)-CRP was reproduced (**Chapter 7**), although its protein of origin is as of yet unclear.

Interestingly, HILIC-UHPLC-FLD and xCGE-LIF allowed new findings on the glycosylation changes occurring with pregnancy and RA disease activity, in the form of branching differences on both monogalactosylated and monoantennary species. With pregnancy, for example, an increased galactosylation was detected of the α 1,6-branch (as opposed to the α 1,3-branch) of nonbisected monogalactosylated FA2, and a decreased α 1,6-branched galactosylation of the bisected variant. The same phenotypes were inversely associated with RA disease activity, principally matching the DAS28(3)-CRP decrease observed with pregnancy²⁹. These observations could be the result of altered glycosyltransferase expression or regulation, but one attractive alternative explanation might be a shift of relative IgG-subclass abundances during pregnancy⁵⁶. As IgG2 and IgG3 display higher α 1,3-branch galactosylation than α 1,6-branch galactosylation, which is contrary to IgG1 and IgG4⁵⁷, the reported relative increase of IgG2 and IgG3 with pregnancy would lead to our observed linkage change in the TSNG^{56,58}.

Table 3. Overview of study results.

Methodology	Information	Advantages	Disadvantages	Sample suitability
HILIC-UHPLC-FLD	Structural	Best repeatability; well-established database; good separation of A2	A3/A4 signal overlap; no novel annotation ^a	Plasma cell glycoproteins or mixtures (immunoglobulins; A2 glycans)
xCGE-LIF	Structural	Throughput due to multiplexing; good separation of A2	A3/A4 signal overlap; no novel annotation ^a	Plasma cell glycoproteins or mixtures (immunoglobulins; A2 glycans)
MALDI-TOF-MS	Compositional; sialic acid linkage	Best throughput; compositional annotation; infrequent signal overlap; good separation of A3/A4; derived traits	Lowest repeatability; no structural information ^a	Hepatic cell glycoproteins (acute phase proteins; A3/A4 glycans); unknown samples

^aAdditional information may be obtained by subsequent experiments such as exoglycosidase sequencing and tandem MS.

8.5 Summary

In summary, we compared the performance of HILIC-UHPLC-FLD, xCGE-LIF and MALDI-TOF-MS for the analysis of the released serum protein *N*-glycome. Next to providing the technical and biological translation between methods, we discussed their advantages and disadvantages, including their respective throughput and repeatability (Table 3). In addition, we explored the differences in information content for various glycosylation types within the TSNG, and speculated upon the suitability of the methods to characterize different sample types. The combined analysis with orthogonal HTP methods proved to be highly informative for the study of the TSNG, and has led, next to confirming previous

findings, to the discovery of new glycosylation traits associated with RA and disease activity thereof.

8.6 Methods

Study population

The research presented here was performed using serum samples from the PARA study, a prospective cohort to study the interaction of pregnancy and RA²⁹. In the current research, serum samples were included from 36 RA patient pregnancies, obtained prior to conception, at the 3rd trimester of pregnancy, and after 26 weeks following partum. At every time point, disease activity was assessed using the 28-joint disease activity score (DAS) with three variables based on the C-reactive protein (CRP) level (mg/L) (DAS28(3)-CRP). In addition, serum samples from 32 apparently healthy pregnancies (without adverse obstetric histories) were included to serve as controls, for these including serum collected at the 3rd trimester of pregnancy and later than 26 weeks post-partum. All pregnancies were completed, and all patients fulfilled the 1987 ACR criteria for RA. The study was in compliance with the Helsinki Declaration and was approved by the Ethics Review Board at the Erasmus University Medical Center, Rotterdam, The Netherlands.

Of each of the 178 clinical samples, 200 μ L serum was distributed in randomized order across two 96-well deep-well plates (polypropylene; NUNC, Rochester, NY). Per plate, an additional 2 positions were filled with phosphate-buffered saline solution to serve as blank, 5 positions with identical plasma as technical standard (Visucon-F frozen normal control plasma; Affinity Biologicals, Ancaster, ON), and 3 positions were left to facilitate the inclusion of standards local to each laboratory. From these master plates, 40 μ L sample was divided into 5 pairs of PCR plates (polypropylene; Greiner Bio-One, Frickenhausen, Germany), which were distributed among the participating laboratories.

HILIC-UHPLC-FLD analysis

Sample preparation and measurement by HILIC-UHPLC-FLD was performed by participants 1, 2 and 3, as previously reported^{23,41,59,60}. The procedures are described in full detail in the supplementary information (respectively **Supplemental Method M1**, **M2**, and **M3**). To summarize, *N*-glycans were released enzymatically from their protein backbones by overnight peptide-*N*-glycosidase F (PNGase F) treatment, labeled with 2-AB by reductive amination, enriched by HILIC solid phase extraction (SPE), and subsequently analyzed by HILIC-UHPLC-FLD. For peak annotation, the sample retention times were calibrated on an external UHPLC run of dextran ladder. The hereby obtained GU values per signal were used to connect to a database of previously established assignments³⁰. Signal numbers were unified between the participants on basis of the structural annotation, principally based on the nomenclature of participant 1.

xCGE-LIF analysis

xCGE-LIF sample preparation and measurement were performed as previously described (**Supplemental Method M4**)^{10,31,61}. Briefly, *N*-glycans were released from the serum proteins by PNGase F, fluorescently labeled by reductive amination with APTS, enriched by HILIC-SPE, and analyzed by a multiplexed capillary gel electrophoresis system with laser-induced fluorescence detection. Each sample was internally calibrated by a co-migrating fluorescent standard, and the resulting migration times were annotated with glycan structures on basis of established database values³¹. Automated migration time normalization, peak picking, integration and database matching were performed by glyXtool³¹.

MALDI-TOF-MS analysis

MALDI-TOF-MS sample preparation and measurement were performed as described previously (**Supplemental Method M5**)^{35,40}. In short, after *N*-glycan release by PNGase F, an automated platform was employed to derivatize the sialic acids by ethyl esterification (of α 2,6-linked sialic acids and lactonization of α 2,3-linked sialic acids), to perform GHP HILIC-SPE, and to spot samples on a MALDI target³⁵. MALDI-TOF-MS analysis was performed in reflectron positive mode, with an accumulation of 10,000 shots per spot in a random walking pattern. Obtained signals were annotated to be $[M+Na]^+$ glycan compositions on basis of the signal-to-noise ratio, the ppm error, and the isotopic ratio.

Data preprocessing and analysis

For each of the methods, signal areas were normalized to the total sum of area per sample (total area normalization). Derived traits were calculated on basis of known enzymatic glycosylation pathways and glycoprotein populations (for derived trait calculations see **Supplemental Table S5**, for a legend describing the derived traits see **Supplemental Table S6**)^{24,28,32-34,37}.

Throughout data analysis, we made use of R 3.1.2 in RStudio 0.98.1091 (RStudio Team, Boston, MA)⁶². The repeatability of each method was assessed by calculating the mean, SD and CV for each signal within the technical control samples (**Supplemental Table S7**). Correlation between glycosylation features in the clinical data was established by calculating the Pearson correlation, and the results hereof were expressed in heat map format (**Figure 2**, **Supplemental Figure S3-S5**). Boxplots and scatterplots were similarly created in R using the total-area-normalized glycosylation values.

For the association analyses with pregnancy, RA and DAS28(3)-CRP, glycosylation (and derived trait) averages were centered to 0, and scaled to represent single SD variations. Pregnancy was defined as binary variable (both preconception and 26+ weeks postpartum = 0; 3rd trimester of pregnancy = 1), as was RA (0 = control, 1 = RA). Mixed logistic regression was employed to test the association of glycosylation (independent) with pregnancy

(dependent), correcting for interindividual effects by assigning a random intercept per individual (**Supplemental Table S8**). Mixed logistic regression was additionally used to test the association between glycosylation (independent) and RA (dependent), correcting for pregnancy by modelling a random intercept per time point (**Supplemental Table S9**). Linear regression was used to test the direct association between glycosylation (independent) and the linear variable DAS28-CRP (dependent), while mixed linear regression was used to differentiate the intraindividual effects (modeling a random intercept per individual) or interindividual effects (modeling a random intercept per time point) (**Supplemental Table S10**).

The study-wide false-discovery rate was controlled to be 5% by application of the Benjamini-Hochberg procedure⁶³, leading to an overall significance threshold of $\alpha = 1.7 \cdot 10^{-2}$ (**Supplemental Table S11**).

Nomenclature

In text, *N*-glycan structures have followed the Oxford nomenclature²³, whereas *N*-glycan compositions have followed H = hexose, N = *N*-acetylhexosamine, F = fucose (deoxyhexose), S = unspecified *N*-acetylneuraminic acid (sialic acid), L = (lactonized) α 2,3-linked *N*-acetylneuraminic acid, and E = (ethyl esterified) α 2,6-linked *N*-acetylneuraminic acid. Figures have been annotated with glycan cartoons following the recommendations of the Consortium for Functional Glycomics⁶⁴ and designed using GlycoWorkbench 2.1 (build 146)⁶⁵.

Acknowledgments

This work was supported by the European Union Seventh Framework Programme project HighGlycan (278535) and the Dutch Arthritis Foundation (NR-10-1-411). Furthermore, we would like to thank Gerda Vreeker, Marco Bladergroen and Yuri van der Burgt for their assistance with measuring the MALDI-TOF-MS data.

8.7 References

- 1 Varki, A. Biological roles of glycans. *Glycobiology* **27**, 3-49, doi:10.1093/glycob/cww086 (2017).
- 2 Hart, G. W. & Copeland, R. J. Glycomics hits the big time. *Cell* **143**, 672-676, doi:10.1016/j.cell.2010.11.008 (2010).
- 3 Thomann, M. *et al.* In vitro glycoengineering of IgG1 and its effect on Fc receptor binding and ADCC activity. *PLoS One* **10**, e0134949, doi:10.1371/journal.pone.0134949 (2015).
- 4 Rouwendal, G. J. *et al.* A comparison of anti-HER2 IgA and IgG1 in vivo efficacy is facilitated by high N-glycan sialylation of the IgA. *MABs* **8**, 74-86, doi:10.1080/19420862.2015.1102812 (2016).
- 5 Oh, M. J. *et al.* Analytical platform for glycomic characterization of recombinant erythropoietin biotherapeutics and biosimilars by MS. *Bioanalysis* **5**, 545-559, doi:10.4155/bio.12.327 (2013).

- 6 Pancera, M. *et al.* Structural basis for diverse N-glycan recognition by HIV-1-neutralizing V1-
V2-directed antibody PG16. *Nat Struct Mol Biol* **20**, 804-813, doi:10.1038/nsmb.2600
(2013).
- 7 von Itzstein, M. *et al.* Rational design of potent sialidase-based inhibitors of influenza virus
replication. *Nature* **363**, 418-423, doi:10.1038/363418a0 (1993).
- 8 Dalziel, M., Crispin, M., Scanlan, C. N., Zitzmann, N. & Dwek, R. A. Emerging principles for
the therapeutic exploitation of glycosylation. *Science* **343**, 1235681,
doi:10.1126/science.1235681 (2014).
- 9 Gornik, O. *et al.* Stability of N-glycan profiles in human plasma. *Glycobiology* **19**, 1547-1553,
doi:10.1093/glycob/cwp134 (2009).
- 10 Hennig, R. *et al.* Towards personalized diagnostics via longitudinal study of the human
plasma N-glycome. *Biochim Biophys Acta* **1860**, 1728-1738,
doi:10.1016/j.bbagen.2016.03.035 (2016).
- 11 Reiding, K. R. *et al.* Human Plasma N-glycosylation as Analyzed by Matrix-Assisted Laser
Desorption/Ionization-Fourier Transform Ion Cyclotron Resonance-MS Associates with
Markers of Inflammation and Metabolic Health. *Mol Cell Proteomics* **16**, 228-242,
doi:10.1074/mcp.M116.065250 (2017).
- 12 Albrecht, S., Unwin, L., Muniyappa, M. & Rudd, P. M. Glycosylation as a marker for
inflammatory arthritis. *Cancer Biomark* **14**, 17-28, doi:10.3233/CBM-130373 (2014).
- 13 Vuckovic, F. *et al.* IgG Glycome in Colorectal Cancer. *Clin Cancer Res* **22**, 3078-3086,
doi:10.1158/1078-0432.CCR-15-1867 (2016).
- 14 Kemna, M. J. *et al.* Galactosylation and Sialylation Levels of IgG Predict Relapse in Patients
With PR3-ANCA Associated Vasculitis. *EBioMedicine* **17**, 108-118,
doi:10.1016/j.ebiom.2017.01.033 (2017).
- 15 Novokmet, M. *et al.* Changes in IgG and total plasma protein glycomes in acute systemic
inflammation. *Sci Rep* **4**, 4347, doi:10.1038/srep04347 (2014).
- 16 Verhelst, X. *et al.* A Glycomics-Based Test Predicts the Development of Hepatocellular
Carcinoma in Cirrhosis. *Clin Cancer Res* **23**, 2750-2758, doi:10.1158/1078-0432.CCR-16-1500
(2017).
- 17 Shubhakar, A. *et al.* High-Throughput Analysis and Automation for Glycomics Studies.
Chromatographia **78**, 321-333, doi:10.1007/s10337-014-2803-9 (2015).
- 18 Gaunitz, S., Nagy, G., Pohl, N. L. & Novotny, M. V. Recent Advances in the Analysis of
Complex Glycoproteins. *Anal Chem* **89**, 389-413, doi:10.1021/acs.analchem.6b04343
(2017).
- 19 Lauc, G. *et al.* Genomics meets glycomics-the first GWAS study of human N-Glycome
identifies HNF1alpha as a master regulator of plasma protein fucosylation. *PLoS Genet* **6**,
e1001256, doi:10.1371/journal.pgen.1001256 (2010).
- 20 Ruhaak, L. R. *et al.* Plasma protein N-glycan profiles are associated with calendar age,
familial longevity and health. *J Proteome Res* **10**, 1667-1674, doi:10.1021/pr1009959 (2011).
- 21 Lauc, G. *et al.* Loci associated with N-glycosylation of human immunoglobulin G show
pleiotropy with autoimmune diseases and haematological cancers. *PLoS Genet* **9**, e1003225,
doi:10.1371/journal.pgen.1003225 (2013).
- 22 Ruhaak, L. R. *et al.* Targeted biomarker discovery by high throughput glycosylation profiling
of human plasma alpha1-antitrypsin and immunoglobulin A. *PLoS One* **8**, e73082,
doi:10.1371/journal.pone.0073082 (2013).
- 23 Saldova, R. *et al.* Association of N-glycosylation with breast carcinoma and systemic features
using high-resolution quantitative UPLC. *J Proteome Res* **13**, 2314-2327,
doi:10.1021/pr401092y (2014).
- 24 Stumpo, K. A. & Reinhold, V. N. The N-glycome of human plasma. *J Proteome Res* **9**, 4823-
4830, doi:10.1021/pr100528k (2010).

- 25 Huffman, J. E. *et al.* Comparative performance of four methods for high-throughput glycosylation analysis of immunoglobulin G in genetic and epidemiological research. *Mol Cell Proteomics* **13**, 1598-1610, doi:10.1074/mcp.M113.037465 (2014).
- 26 Reusch, D. *et al.* Comparison of methods for the analysis of therapeutic immunoglobulin G Fc-glycosylation profiles--part 1: separation-based methods. *MAbs* **7**, 167-179, doi:10.4161/19420862.2014.986000 (2015).
- 27 Reusch, D. *et al.* Comparison of methods for the analysis of therapeutic immunoglobulin G Fc-glycosylation profiles-Part 2: Mass spectrometric methods. *MAbs* **7**, 732-742, doi:10.1080/19420862.2015.1045173 (2015).
- 28 Clerc, F. *et al.* Human plasma protein N-glycosylation. *Glycoconj J* **33**, 309-343, doi:10.1007/s10719-015-9626-2 (2016).
- 29 de Man, Y. A., Dolhain, R. J., van de Geijn, F. E., Willemsen, S. P. & Hazes, J. M. Disease activity of rheumatoid arthritis during pregnancy: results from a nationwide prospective study. *Arthritis Rheum* **59**, 1241-1248, doi:10.1002/art.24003 (2008).
- 30 Campbell, M. P., Royle, L., Radcliffe, C. M., Dwek, R. A. & Rudd, P. M. GlycoBase and autoGU: tools for HPLC-based glycan analysis. *Bioinformatics* **24**, 1214-1216, doi:10.1093/bioinformatics/btn090 (2008).
- 31 Hennig, R., Reichl, U. & Rapp, E. A software tool for automated high-throughput processing of CGE-LIF based glycoanalysis data, generated by a multiplexing capillary DNA sequencer. *Glycoconj J* **28**, 331 (2011).
- 32 Nairn, A. V. *et al.* Regulation of glycan structures in animal tissues: transcript profiling of glycan-related genes. *J Biol Chem* **283**, 17298-17313, doi:10.1074/jbc.M801964200 (2008).
- 33 Freeze, H. H. Genetic defects in the human glycome. *Nat Rev Genet* **7**, 537-551, doi:10.1038/nrg1894 (2006).
- 34 Kang, P., Mechref, Y. & Novotny, M. V. High-throughput solid-phase permethylation of glycans prior to mass spectrometry. *Rapid Commun Mass Spectrom* **22**, 721-734, doi:10.1002/rcm.3395 (2008).
- 35 Bladergroen, M. R. *et al.* Automation of High-Throughput Mass Spectrometry-Based Plasma N-Glycome Analysis with Linkage-Specific Sialic Acid Esterification. *J Proteome Res* **14**, 4080-4086, doi:10.1021/acs.jproteome.5b00538 (2015).
- 36 Leymarie, N. *et al.* Interlaboratory study on differential analysis of protein glycosylation by mass spectrometry: the ABRF glycoprotein research multi-institutional study 2012. *Mol Cell Proteomics* **12**, 2935-2951, doi:10.1074/mcp.M113.030643 (2013).
- 37 Klein, A. Human total serum N-glycome. *Adv Clin Chem* **46**, 51-85 (2008).
- 38 Hemstrom, P. & Irgum, K. Hydrophilic interaction chromatography. *J Sep Sci* **29**, 1784-1821 (2006).
- 39 Callewaert, N., Geysens, S., Molemans, F. & Contreras, R. Ultrasensitive profiling and sequencing of N-linked oligosaccharides using standard DNA-sequencing equipment. *Glycobiology* **11**, 275-281 (2001).
- 40 Reiding, K. R., Blank, D., Kuijper, D. M., Deelder, A. M. & Wuhrer, M. High-throughput profiling of protein N-glycosylation by MALDI-TOF-MS employing linkage-specific sialic acid esterification. *Anal Chem* **86**, 5784-5793, doi:10.1021/ac500335t (2014).
- 41 Stockmann, H., O'Flaherty, R., Adamczyk, B., Saldova, R. & Rudd, P. M. Automated, high-throughput serum glycoproteomic platform. *Integr Biol (Camb)* **7**, 1026-1032, doi:10.1039/c5ib00130g (2015).
- 42 Gong, B. *et al.* N-glycosylamine-mediated isotope labeling for mass spectrometry-based quantitative analysis of N-linked glycans. *Anal Bioanal Chem* **405**, 5825-5831, doi:10.1007/s00216-013-6988-9 (2013).
- 43 Alvarez-Manilla, G. *et al.* Tools for glycomics: relative quantitation of glycans by isotopic permethylation using ¹³CH₃I. *Glycobiology* **17**, 677-687, doi:10.1093/glycob/cwm033 (2007).

- 44 Zhou, S., Dong, X., Veillon, L., Huang, Y. & Mechref, Y. LC-MS/MS analysis of permethylated N-glycans facilitating isomeric characterization. *Anal Bioanal Chem* **409**, 453-466, doi:10.1007/s00216-016-9996-8 (2017).
- 45 Zhong, X. *et al.* Capillary Electrophoresis-Electrospray Ionization-Mass Spectrometry for Quantitative Analysis of Glycans Labeled with Multiplex Carbonyl-Reactive Tandem Mass Tags. *Anal Chem* **87**, 6527-6534, doi:10.1021/acs.analchem.5b01835 (2015).
- 46 Guttman, M. & Lee, K. K. Site-Specific Mapping of Sialic Acid Linkage Isomers by Ion Mobility Spectrometry. *Anal Chem* **88**, 5212-5217, doi:10.1021/acs.analchem.6b00265 (2016).
- 47 Jansen, B. C. *et al.* Pregnancy-associated serum N-glycome changes studied by high-throughput MALDI-TOF-MS. *Sci Rep* **6**, 23296, doi:10.1038/srep23296 (2016).
- 48 Ruhaak, L. R., Uh, H. W., Deelder, A. M., Dolhain, R. E. & Wuhrer, M. Total plasma N-glycome changes during pregnancy. *J Proteome Res* **13**, 1657-1668, doi:10.1021/pr401128j (2014).
- 49 Parekh, R. B. *et al.* Association of rheumatoid arthritis and primary osteoarthritis with changes in the glycosylation pattern of total serum IgG. *Nature* **316**, 452-457 (1985).
- 50 Bondt, A. *et al.* Association between galactosylation of immunoglobulin G and improvement of rheumatoid arthritis during pregnancy is independent of sialylation. *J Proteome Res* **12**, 4522-4531, doi:10.1021/pr400589m (2013).
- 51 Bondt, A. *et al.* Immunoglobulin G (IgG) Fab glycosylation analysis using a new mass spectrometric high-throughput profiling method reveals pregnancy-associated changes. *Mol Cell Proteomics* **13**, 3029-3039, doi:10.1074/mcp.M114.039537 (2014).
- 52 Brinkman-van der Linden, E. C., de Haan, P. F., Havenaar, E. C. & van Dijk, W. Inflammation-induced expression of sialyl LewisX is not restricted to alpha1-acid glycoprotein but also occurs to a lesser extent on alpha1-antichymotrypsin and haptoglobin. *Glycoconj J* **15**, 177-182 (1998).
- 53 Havenaar, E. C. *et al.* Severe rheumatoid arthritis prohibits the pregnancy-induced decrease in alpha3-fucosylation of alpha1-acid glycoprotein. *Glycoconj J* **15**, 723-729 (1998).
- 54 Kolarich, D., Weber, A., Turecek, P. L., Schwarz, H. P. & Altmann, F. Comprehensive glycoproteomic analysis of human alpha1-antitrypsin and its charge isoforms. *Proteomics* **6**, 3369-3380, doi:10.1002/pmic.200500751 (2006).
- 55 Lee, J. Y. *et al.* Characterization of Site-Specific N-Glycopeptide Isoforms of alpha-1-Acid Glycoprotein from an Interlaboratory Study Using LC-MS/MS. *J Proteome Res* **15**, 4146-4164, doi:10.1021/acs.jproteome.5b01159 (2016).
- 56 Wilson, R. *et al.* Abnormal immunoglobulin subclass patterns in women with a history of recurrent miscarriage. *Fertil Steril* **76**, 915-917 (2001).
- 57 Jefferis, R. *et al.* A comparative study of the N-linked oligosaccharide structures of human IgG subclass proteins. *Biochem J* **268**, 529-537 (1990).
- 58 Larsson, A., Palm, M., Hansson, L. O., Basu, S. & Axelsson, O. Reference values for alpha1-acid glycoprotein, alpha1-antitrypsin, albumin, haptoglobin, C-reactive protein, IgA, IgG and IgM during pregnancy. *Acta Obstet Gynecol Scand* **87**, 1084-1088, doi:10.1080/00016340802428146 (2008).
- 59 Akmacic, I. T. *et al.* High-throughput glycomics: optimization of sample preparation. *Biochemistry (Mosc)* **80**, 934-942, doi:10.1134/S0006297915070123 (2015).
- 60 Adamczyk, B., Stockmann, H., O'Flaherty, R., Karlsson, N. G. & Rudd, P. M. High-Throughput Analysis of the Plasma N-Glycome by UHPLC. *Methods Mol Biol* **1503**, 97-108, doi:10.1007/978-1-4939-6493-2_8 (2017).
- 61 Hennig, R. *et al.* N-Glycosylation Fingerprinting of Viral Glycoproteins by xCGE-LIF. *Methods Mol Biol* **1331**, 123-143, doi:10.1007/978-1-4939-2874-3_8 (2015).
- 62 RCore Team. R: a language and environment for statistical computing. R Foundation for Statistical Computing, Vienna, Austria. <http://www.R-project.org/>. (2014).
- 63 Benjamini, Y. & Hochberg, Y. Controlling the False Discovery Rate - a Practical and Powerful Approach to Multiple Testing. *J Roy Stat Soc B Met* **57**, 289-300 (1995).

- 64 Varki, A. *et al.* Symbol Nomenclature for Graphical Representations of Glycans. *Glycobiology* **25**, 1323-1324, doi:10.1093/glycob/cwv091 (2015).
- 65 Ceroni, A. *et al.* GlycoWorkbench: a tool for the computer-assisted annotation of mass spectra of glycans. *J Proteome Res* **7**, 1650-1659, doi:10.1021/pr7008252 (2008).
- 66 Ventham, N. T. *et al.* Changes to serum sample tube and processing methodology does not cause Intra-Individual [corrected] variation in automated whole serum N-glycan profiling in health and disease. *PLoS One* **10**, e0123028, doi:10.1371/journal.pone.0123028 (2015).